

# Semiclassical Klein Tunneling and Valley Hall Effect in Graphene

Christoph M. Puetter,<sup>1,\*</sup> Satoru Konabe,<sup>1,2</sup> Yasuhiro Tokura,<sup>1</sup> Yasuhiro Hatsugai,<sup>1,3</sup> and Kenji Shiraishi<sup>4,1,3</sup>

<sup>1</sup>*Graduate School of Pure and Applied Sciences, University of Tsukuba, 1-1-1 Tennodai, Tsukuba, 305-8577, Japan*

<sup>2</sup>*CREST, Japan Science and Technology Agency, 4-1-8 Honcho Kawaguchi, 332-0012, Japan*

<sup>3</sup>*Center for Integrated Electronic Systems, Tohoku University, Sendai 980-8578, Japan*

<sup>4</sup>*Graduate School of Engineering, Nagoya University, Nagoya, 464-8603, Japan*

We study the dynamics of semiclassical electrons in (gapped) graphene in two complementary limits, i.e. in the Klein tunneling and valley Hall effect regimes, by scattering wave packets off armchair step potentials and by exposing wave packets to a uniform electric field, respectively. Our numerical wave packet simulation goes beyond semiclassical analytical approximations and standard Klein tunneling treatments and allows to study intra- and intervalley scattering processes. We find distinct Klein tunneling characteristics for low and tall steps, which include unusual Berry curvature induced side shifts of the scattered wave packet trajectories. In the presence of a uniform field, our simulations capture the semiclassical valley Hall effect which manifests in the form of laterally shifted Bloch oscillations. Such anomalous trajectory corrections can be relevant for Klein tunneling experiments and electron optics devices. We present detailed simulation results.

PACS numbers: 72.80.Vp

## I. INTRODUCTION

Graphene possesses extraordinary electronic transport properties due to the two special points in the band structure where conduction and valence band meet. At these so-called Dirac points the energy dispersion is conical, and electrons circling around each Dirac point acquire a nontrivial Berry phase of  $\pm\pi$ .<sup>1</sup> A nontrivial Berry phase can lead to remarkable transport phenomena as displayed by the half-integer quantum Hall effect in graphene<sup>2-4</sup> and the intrinsic anomalous Hall effect in ferromagnetic materials.<sup>5</sup> The valley Hall effect and the Klein paradox, too, are closely associated with the conical Dirac dispersion. In gapped graphene and related materials such as silicene and germanene,<sup>6-10</sup> both the valley Hall effect and the Klein paradox can provide striking signatures of the underlying nontrivial band topologies and, in general, involve both Dirac valleys.

The Klein paradox refers to the almost certain transmission of relativistic Dirac fermions across a potential barrier regardless of its height and width.<sup>11</sup> Considerable effort has recently been put into observing and exploring the Klein phenomenon in graphene devices,<sup>12-19</sup> with evidence reported based on resistance measurements across a potential barrier and comparison with theoretical predictions for ballistic and diffusive transport;<sup>15</sup> conductance oscillations across a potential barrier;<sup>16</sup> and characteristic angle-selective transmission at pn junctions.<sup>18,19</sup> In contrast, the valley Hall effect occurs in the opposite limit where a sharp step potential or barrier potential is replaced by a uniform potential gradient, leading to electronic Bloch oscillations in ideal dissipationless systems. Valley-based phenomena have recently attracted particular interest due to the technological potential of spin-valley selective photoelectric excitations in the quasi-2D transition metal dichalcogenides.<sup>20-24</sup>

In the present paper we utilize a semiclassical wave packet simulation. A semiclassical approximation can

provide unique insight into the effective dynamics of Bloch electrons in bands with nontrivial topologies.<sup>25,26</sup> This is evident from the semiclassical equations of motion

$$\dot{\mathbf{r}} = \nabla_{\mathbf{k}} \epsilon_{\mathbf{k}} - \dot{\mathbf{k}} \times \hat{\Omega}_{\mathbf{k}}, \quad \dot{\mathbf{k}} = -e(\mathbf{E} + \dot{\mathbf{r}} \times \mathbf{B}), \quad (1)$$

where  $\mathbf{r}$  stands for the electron position,  $\epsilon_{\mathbf{k}}$  for the band energy at crystal momentum  $\mathbf{k}$ ,  $e$  for the elementary charge,  $\mathbf{E}$  and  $\mathbf{B}$  for electric and magnetic field, respectively, while, crucially, the first cross product term represents a correction due to the Berry curvature  $\hat{\Omega}_{\mathbf{k}}$  and the driving force  $\dot{\mathbf{k}}$ . A wave packet simulation has further advantages. It goes beyond the standard analytical treatment of Klein tunneling in graphene, which usually relies on linearized single valley Dirac bands and a plane wave ansatz, and hence is insufficient to capture intervalley scattering and Berry phase related effects.<sup>27-30</sup> In addition, in contrast to the semiclassical analytical formalism [exemplified by Eq. (1)], which requires smooth fields, single or degenerate bands and uniquely defined wave packet centres in real space and in momentum space,<sup>25,31</sup> a wave packet simulation is in principle exact and generalizes the semiclassical approach to arbitrary potentials and multi-band systems.

For simplicity we focus on the dynamics of semiclassical spinless electrons in the Klein tunneling and valley Hall effect regimes, by scattering wave packets off armchair potential steps and by imposing a smooth potential gradient, respectively, while taking the full graphene tight-binding Hamiltonian into account. Our main findings are two-fold. First, our numerical study reveals distinct Berry curvature induced side shifts in the wave packet motion near potential steps [see Fig. 1 (a)] that are direct, two-dimensional analogues of those appearing in the optical Hall effect.<sup>32,33</sup> These shifts occur even in the sharp step limit where the driving force is almost singularly confined to the step edge and indicate deviations from simple reflection and refraction laws. Since we account for the full dispersion, the transmission and

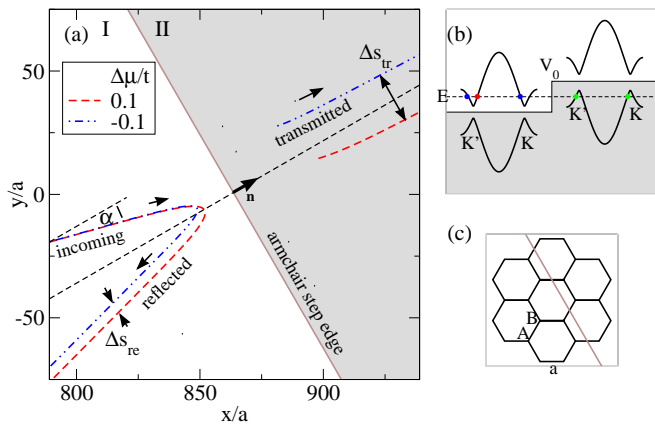


FIG. 1. (Color online) (a) Wave packet trajectories for different staggered sublattice potentials ( $\Delta\mu = \pm 0.1t$ ) yielding different Berry curvatures. The step edge and step normal are indicated by the solid brown and dashed black lines, respectively, while region I (II) mark the lower (upper) portions of the step where  $V(\mathbf{r}) = 0$  ( $V_0$ ). Here the step is sharp, i.e.  $\Delta w = 0$ . The trajectories near the step edge are in general not well defined and have been omitted for the transmitted wave packet portions for clarity. (b) Schematic of the Klein tunneling energy-momentum relation at an armchair potential step. (c) Orientation of the armchair edge (brown line) on the graphene lattice. See main text for details.

reflection probabilities, in addition to the lateral shifts, vary with height and width of the potential step. This behavior is a consequence of distinct intra- and intervalley scattering regimes and give rise to substantial corrections to the usual Klein tunneling process for relativistic Dirac particles.<sup>11,29,30</sup>

Second, in the opposite case of an extended linear potential, we find Bloch-Zener oscillations that acquire a finite component perpendicular to the potential gradient (see Fig. 2). These modified oscillations are a manifestation of the valley Hall effect where the trajectory side shifts are induced by a finite Berry curvature near the Dirac points.<sup>25,34</sup> The present simulations allow to investigate in detail the accompanying interband Bloch-Zener transitions that occur near the Dirac points and are closely related to the transmitted wave packet portions in the Klein tunneling regime. The interband transitions lead to two wave packet portions with opposite velocities and trajectories as indicated e.g. by the two red solid lines in Fig. 2.

The paper is organized as follows. In Sec. II we introduce the model, the simulation details and useful definitions. In Sec. III we present the results for semiclassical Klein tunneling at sharp and smooth potential steps using the full graphene tight-binding Hamiltonian. To illuminate the basic intra- and inter-valley scattering processes, the first subsection (III A) discusses in detail the transmission and reflection probabilities and their valley affiliations. The second subsection (III B) focusses on the lateral trajectory shifts induced near a step interface by a finite Berry curvature. Sec. IV is devoted to the

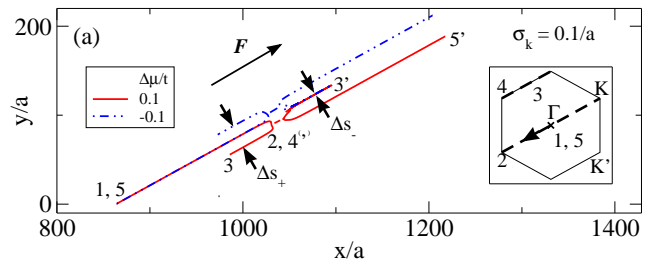


FIG. 2. (Color online) Bloch oscillations / valley Hall effect of wave packets in the presence of a uniform electric field with magnitude  $F = 0.015 t / (|e|a)$ . The main panel shows the real space wave packet trajectories of electron and hole band portions for different staggered sublattice potentials ( $\Delta\mu = \pm 0.1t$ ). The inset displays the corresponding trajectory in momentum space. The numbers in the main panel and in the inset correspond to each other and indicate temporal order. See main text for details.

semiclassical valley Hall effect. Here we apply a uniform potential gradient and present the simulation results for the wave packet Bloch oscillations and the accompanying trajectory side shifts. The last section closes with a summary and a brief discussion of the findings.

## II. SEMICLASSICAL WAVE PACKET PROPAGATION

To study the semiclassical single electron dynamics we consider a spinless electron wave packet moving in a two-dimensional honeycomb lattice towards a potential step. Although it is experimentally challenging to fabricate graphene devices with thin junction interfaces,<sup>13</sup> a narrow potential step is the simplest setup and an instructive limit to investigate semiclassical Klein tunneling on a lattice. In addition, narrow potential steps may also arise accidentally from the presence of impurities or imperfections of the underlying substrate. We contrast the Klein tunneling scattering dynamics at a potential step with the Bloch-Zener oscillation dynamics in the presence of an extended linear potential, which can be imposed by applying a bias voltage. A staggered sublattice potential, which opens an energy gap and leads to a finite Berry curvature near the Dirac points, may be induced by an adequate substrate, or, in the case of related buckled quasi-two-dimensional materials like silicene or germanene, by applying a perpendicular electric field. In the latter materials, however, a splitting of the Bloch bands due to significant spin-orbit interaction needs to be taken into account.<sup>9</sup>

In the simulation the time evolution of the wave packet  $|\psi(\tau)\rangle$  is governed by the time-dependent Schroedinger equation  $i\partial_\tau|\psi(\tau)\rangle = (H_0 + H_V)|\psi(\tau)\rangle$ , which contains

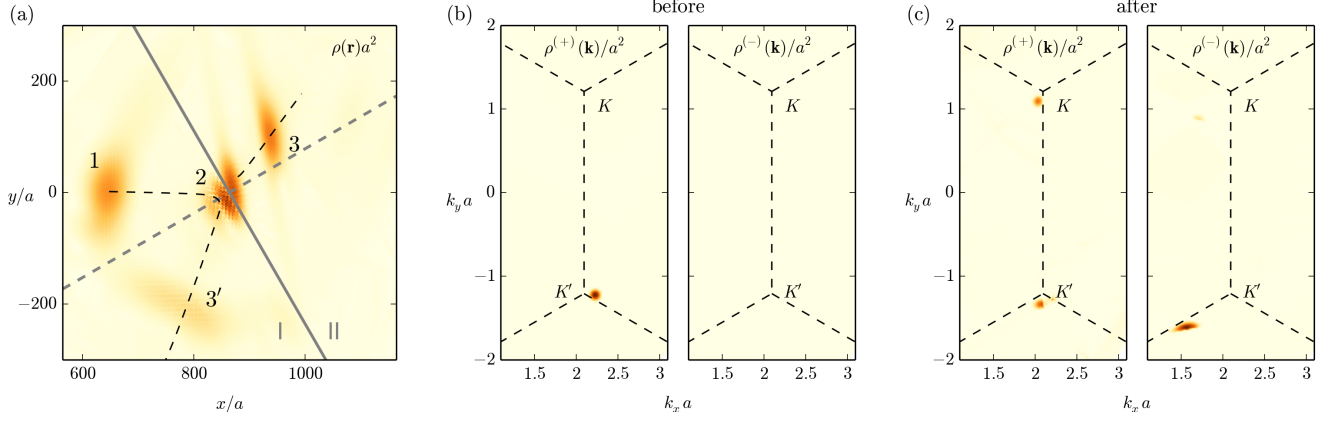


FIG. 3. (Color online) (a) Real space snapshot sequence of a wave packet scattering at an armchair step potential (indicated by the grey solid line) before (1), at (2) and after scattering (3, 3'). After scattering the wave function consists of transmitted (3) and reflected (3') portions. The grey dashed line is normal to the step edge, while the black dashed lines indicate the centre of mass trajectories in regions I and II. (b) Initial momentum space snapshot corresponding to instance 1 in panel (a). Only electron states near  $K'$  contribute to the wave packet composition. (c) Momentum space snapshot after scattering representing instance {3, 3'} [see panel (a)]. The transmitted (3) portion's major (minor) contribution stems from the hole band near  $K'$  ( $K$ ), while the reflected (3') wave packet portion has contributions from electron states near both  $K$  and  $K'$ . See main text for details.

the usual honeycomb tight-binding Hamiltonian<sup>1</sup>

$$H_0 = -t \sum_{\mathbf{r}} (c_{\mathbf{r}}^{a\dagger} c_{\mathbf{r}}^b + c_{\mathbf{r}}^{a\dagger} c_{\mathbf{r}-\mathbf{a}_1}^b + c_{\mathbf{r}}^{a\dagger} c_{\mathbf{r}-\mathbf{a}_1+\mathbf{a}_2}^b + \text{h. c.}) + \Delta\mu \sum_{\mathbf{r}} (c_{\mathbf{r}}^{a\dagger} c_{\mathbf{r}}^a - c_{\mathbf{r}}^{b\dagger} c_{\mathbf{r}}^b) \quad (2)$$

and the external potential

$$H_V = \sum_{\mathbf{r}} [V(\mathbf{r})c_{\mathbf{r}}^{a\dagger} c_{\mathbf{r}}^a + V(\mathbf{r} + \vec{\delta})c_{\mathbf{r}}^{b\dagger} c_{\mathbf{r}}^b]. \quad (3)$$

Here  $t$  denotes the nearest-neighbor hopping integral,  $\mathbf{a}_1$  and  $\mathbf{a}_2$  the lattice vectors and  $\Delta\mu$  the staggered sublattice potential. In the following, the external potential  $V(\mathbf{r}) = V_0 g[\mathbf{n} \cdot (\mathbf{r} - \mathbf{r}_0)]$  either represents a potential step of height  $V_0$ , location  $\mathbf{r}_0$  and step normal direction  $\mathbf{n}$  [see Fig. 1 (a)] or a linear electric potential  $V(\mathbf{r}) = -e \mathbf{F} \cdot \mathbf{r}$  with field  $\mathbf{F}$  and electron charge  $e (< 0)$ . The potential step profile is given by

$$g(x) = \begin{cases} 0, & x < -\frac{\Delta w}{2} \\ \left(\frac{1}{2} + \frac{x}{\Delta w}\right), & -\frac{\Delta w}{2} \leq x \leq \frac{\Delta w}{2} \\ 1, & \frac{\Delta w}{2} < x \end{cases}, \quad (4)$$

where  $\Delta w$  denotes the step width [if  $\Delta w = 0$  then  $g(x) = a \delta(x)$ , where  $a$  is the nearest-neighbor distance], The operator  $c_{\mathbf{r}}^{a\dagger}$  ( $c_{\mathbf{r}}^{b\dagger}$ ) creates an electron on sublattice A (B) in unit cell  $\mathbf{r}$ , while  $\vec{\delta}$  denotes the intra-unit cell nearest-neighbor vector.

The wave packet evolution then follows straightforwardly from a fourth order split-operator (Suzuki-Trotter) approximation scheme  $|\psi(\tau)\rangle \approx \Pi_{n=1}^N e^{-iH\Delta\tau} |\psi(\tau=0)\rangle$ , where  $\Delta\tau = \tau/N$  and  $N$  is the total number of iterations.<sup>35,36</sup> For simplicity, we impose

periodic boundary conditions and use sufficiently large system sizes and small enough time steps to reduce finite size effects. Although we evolve the wave packet numerically using the real space representation, i.e.

$$|\psi(\tau)\rangle = \sum_{\mathbf{r}} [\Psi_A(\mathbf{r}; \tau) c_{\mathbf{r}}^{a\dagger} + \Psi_B(\mathbf{r}; \tau) c_{\mathbf{r}}^{b\dagger}] |0\rangle, \quad (5)$$

where  $\Psi_{A(B)}(\mathbf{r}; \tau)$  stands for the wave function on sublattice A (B), it is convenient to specify the initial wave packet at  $\tau = 0$  using the eigenbasis of the  $H_0$ . Thus in the following the initial wave packet is given as a Gaussian-like superposition of positive energy eigenstates centered close to the  $K'$  Dirac point [see Fig. 3 (b)]

$$|\psi(\tau=0)\rangle = \sum_{\mathbf{k}} \Psi_{\mathbf{k}_0, \sigma_k, \mathbf{r}_0}^{(+)}(\mathbf{k}) \xi_{\mathbf{k}}^{(+)\dagger} |0\rangle, \quad (6)$$

where  $\xi_{\mathbf{k}}^{(+)\dagger}$  creates a state with momentum  $\mathbf{k}$  in the electron band. The momentum distribution  $\Psi_{\mathbf{k}_0, \sigma_k, \mathbf{r}_0}^{(+)}(\mathbf{k})$  is centered at  $\mathbf{k}_0$  (which, if not stated otherwise, lies close to  $K'$ ) and characterized by a width  $\sigma_k$ , while the initial position in real space is determined through  $\mathbf{r}_0$ .<sup>37</sup> Initializing the wave packet using states from both electron and hole bands would complicate the propagation dynamics as additional interference phenomena such as trembling motion (*Zitterbewegung*) may appear.<sup>38-40</sup>

Significant dispersion of free wave packets with central momenta near the Dirac points<sup>41</sup> hampers the identification of transmitted and reflected trajectory shifts close to the step edge. To prevent such a complication, we choose the phase of  $\Psi_{\mathbf{k}_0, \sigma_k, \mathbf{r}_0}^{(+)}(\mathbf{k})$  such that the real space wave packet is most compact and symmetric at the point of impact onto the step edge (see Fig. 3), which is roughly

given by  $\mathbf{r}_0$ . The precise definition of  $\Psi_{\mathbf{k}_0, \sigma_k, \mathbf{r}_0}^{(+)}(\mathbf{k})$  is provided in Ref. 37.

### III. SEMICLASSICAL KLEIN TUNNELING AT AN ARMCHAIR STEP EDGE

In this part we investigate the scattering of wave packets at sharp and smooth armchair steps with variable step heights, step widths and wave packet sizes. For an incoming wave packet with a central momentum close to the  $K'$  valley, the armchair edge is distinct from other edge orientations as scattering in general involves states from both  $K$  and  $K'$  points. A consequence is that the transmission (reflection) probability does not increase (decrease) monotonously with the step height as in the standard Klein tunneling problem with a single, strictly linear Dirac valley.<sup>30</sup> In addition, opening a gap by a staggered sublattice potential induces a finite Berry curvature that, as shown below, can affect outgoing wave packet trajectories and breaks pseudospin conservation.

The typical real and momentum space evolution of a wave packet scattering off an armchair step potential is shown in Fig. 3. Panel (a) displays the real space probability distribution of the wave packet  $\rho(\mathbf{r}; \tau) = |\Psi_A(\mathbf{r}; \tau)|^2 + |\Psi_B(\mathbf{r}; \tau)|^2$  at three time instances  $\tau = 0, 160 t^{-1}$  and  $300 t^{-1}$ ; in addition, panels (b) and (c) indicate the corresponding momentum space distributions  $\rho^{(\pm)}(\mathbf{k}; \tau) = |\Psi^{(\pm)}(\mathbf{k}; \tau)|^2$  in electron and hole bands before ( $\tau = 0$ ) and after ( $300 t^{-1}$ ) scattering, respectively. The wave functions  $\Psi_{A/B}(\mathbf{r}; \tau)$  and  $\Psi^{(\pm)}(\mathbf{k}; \tau)$  are related by a unitary transformation that diagonalizes  $H_0$ . The step height, the step width, the energy and the initial momentum space size of the wave packet are  $V_0 = 2.0t$ ,  $\Delta w = 0$ ,  $E = 0.2t$  and  $\sigma_k = 0.1/a$ , respectively. The states contributing to the initial wave packet are located near the  $K'$  valley and have positive energy [see left-hand side of panel (b)]. Upon impact onto the step edge, the wave packet splits and is partially transmitted and partially reflected. The Klein tunneling process involves an interband transition from the electron band to the hole band, which causes the appearance of a nonzero weight on the right-hand side in panel (c). Furthermore, the left-hand side of panel (c) clearly indicates that, for the present parameters, the reflected wave packet portion consists of contributions from both Dirac valleys. Such behaviour is allowed by energy and momentum conservation and is expected to occur at narrow armchair steps. More generally, both transmitted and reflected wave packet portions can have contributions from  $K$  and  $K'$  as indicated in Fig. 1 (b), where the energy-momentum of the incoming wave packet is indicated in red and the outgoing energy-momenta are marked in green (transmitted portion) and blue (reflected portion).

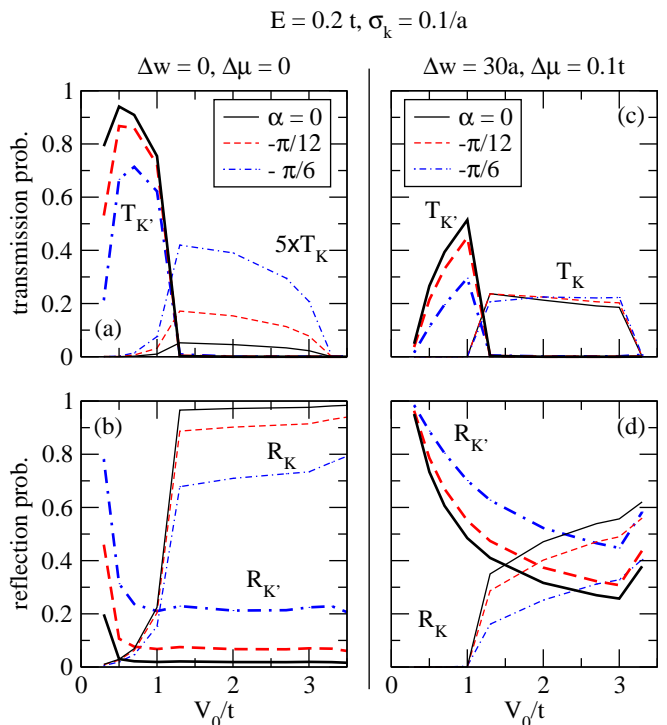


FIG. 4. (Color online) Valley-resolved transmission ( $T_K, T_{K'}$ ) and reflection ( $R_K, R_{K'}$ ) probabilities for an incoming wave packet of energy  $E$  and size  $\sigma_k$  scattering at an armchair step edge as a function of step height  $V_0$ . Thick (thin) lines represent the  $K'$  ( $K$ ) valley. The parameter  $\alpha$  denotes the angle of the incoming trajectory relative to the step normal [see Fig. 1 (a)]. On the left-hand side the step width  $\Delta w$  vanishes and the bands are gapless ( $\Delta\mu = 0$ ). On the right-hand side the step width is finite but narrow and the band structure exhibits a finite gap. In (a) the curves for  $T_K$  have been multiplied by factor of 5 for better visibility.

#### A. Intra- and intervalley scattering

Before turning to the lateral shifts associated with reflection and transmission at the step edge, it is useful to consider the reflection and transmission probabilities of the Klein tunneling process in more detail. These are shown in the Fig. 4, where panels (a) and (b) display the valley-resolved transmission and reflection probabilities, respectively, for a sharp step ( $\Delta w = 0$ ) in the absence of a staggered sublattice potential ( $\Delta\mu = 0$ ). Since for sufficiently large steps ( $V_0 > E$ ), the transmitted and the reflected wave packet portions belong to the hole and the electron band, respectively, the valley-resolved transmission and reflection probabilities are simply defined by

$$T_\nu = \sum_{\mathbf{k} \in \text{BZ}_\nu} \rho^{(-)}(\mathbf{k}; \tau'), \quad R_\nu = \sum_{\mathbf{k} \in \text{BZ}_\nu} \rho^{(+)}(\mathbf{k}; \tau'), \quad (7)$$

where  $\nu = K, K'$  and the set  $\text{BZ}_K$  contains all momenta of the first Brillouin zone that are closer to  $K$  than  $K'$  and vice versa for  $\text{BZ}_{K'}$ . The conservation of probability implies  $T_K + T_{K'} + R_K + R_{K'} = 1$ . The time  $\tau'$  is chosen

sufficiently large so that transmitted and reflected real space wave packet portions are well removed from the step edge.

Clearly, transmission and reflection are drastically different for low and high step heights  $V_0$  and vary with incoming angle  $\alpha$  [see Fig. 1 (a)]. At low step heights  $V_0 \lesssim V_c$ , where  $V_c = t + E = 1.2t$ , the scattering of the wave packets in Fig. 4 is dominated by the  $K'$  valley where the initial wave packet momentum is located. At larger steps  $V_0 \gtrsim V_c$ , intervalley scattering dominates. Particularly notable is the effect of pseudospin conservation,<sup>30</sup> which suppresses transmission for  $V_0 \gtrsim V_c$  and therefore enhances intervalley reflection. For step heights greater than  $V_0 \gtrsim 3t + E (= 3.2t)$ , transmission is completely suppressed since no states are energetically accessible in region II. The suppression of  $T_{K'}$  at  $V_0 \approx 1.2t$  has a similar origin as the  $K'$  valley cannot provide states with suitable momenta and energy for transmission [see also Fig. 1 (b)].

The panels (c) and (d) of Fig. 4 display the effect of a finite gap  $\Delta\mu \neq 0$  and a smooth ( $\Delta w \neq 0$ ) potential step. Qualitatively, the dependencies of transmission and reflection probabilities on  $V_0$  and  $\alpha$  are similar to the  $\Delta\mu = 0$  and  $\Delta w = 0$  case. However, the main effect of widening the step and/or inducing a gap is the enhanced (reduced) transmission at high (low) step heights, i.e. increased  $T_K$  (decreased  $T_{K'}$ ). This observation even applies when varying  $\Delta\mu$  and  $\Delta w$  independently and is consistent with the lack of pseudospin conservation for finite  $\Delta\mu$  and  $\Delta w$ . Due to the narrow step width, the Klein tunneling process here can be considered as a nonadiabatic Landau-Zener interband transition, where the transition probability usually depends sensitively on the transition time (given by the potential gradient) and the gap size.<sup>42–44</sup>

## B. Berry curvature induced lateral shifts

Since we are concerned with a single step only, we define the trajectories on either side of the step profile via

$$\mathbf{r}_M = \sum_{\mathbf{r} \in M} \mathbf{r} |\Psi_A(\mathbf{r}; \tau)|^2 + \sum_{\mathbf{r} + \vec{\delta} \in M} (\mathbf{r} + \vec{\delta}) |\Psi_B(\mathbf{r}; \tau)|^2, \quad (8)$$

where  $M = \text{I, II}$  and the regions I and II are indicated in Fig. 1 (a). This trajectory definition is only well defined when the wave function portions on either side are sufficiently removed from the step interface. For this reason the transmitted wave packet trajectories in Fig. 1 (a) in region II are partially omitted for clarity. To compute the Berry curvature induced lateral shifts, we utilize only the trajectory sections far away from the step interface.

To quantify the lateral shifts of the outgoing (asymptotic) trajectories due to the anomalous velocity term in the semiclassical equation of motions and to clarify that these shifts arise dominantly from the Berry curvature  $\hat{\Omega}_{\mathbf{k}}$ , we plot the differences of the shifts occurring

for positive and negative effective mass as a function of  $|\Delta\mu|$  in Fig. 5. The sign of the Berry curvature, which depends on the sign of  $\Delta\mu$  does not affect the energy dispersion. Hence incoming and outgoing wave packet energies, momenta and group velocities remain unaltered under such a sign change. However, the topological properties of the Bloch wave functions change, and therefore any accompanying changes in the wave packet trajectories [see Fig. 1 (a)] are due to a change of  $\hat{\Omega}_{\mathbf{k}}$ . The Berry curvature for electron and hole bands of  $H_0$  can be determined explicitly<sup>34</sup> and simplifies near the Dirac points ( $|\mathbf{q}| \ll |\mathbf{K}|, |\mathbf{K}'|$ ) to<sup>45</sup>

$$\hat{\Omega}_{\mathbf{K}+\mathbf{q}}^\nu \approx \nu \frac{9a^2 t^2 \Delta\mu}{[4\Delta\mu^2 + 9|\mathbf{q}|^2 a^2 t^2]^{3/2}} \hat{\mathbf{z}}, \quad (9)$$

$$\hat{\Omega}_{\mathbf{K}'+\mathbf{q}}^\nu = -\hat{\Omega}_{\mathbf{K}+\mathbf{q}}^\nu, \quad (10)$$

where  $\nu = \pm$  stands for the band index.

The lateral shifts in Fig. 5 are defined as the projected shifts parallel to the armchair step edge

$$\Delta s_{\text{tr}}(|\Delta\mu|) = \mathbf{s}_{\text{re}}(|\Delta\mu|) - \mathbf{s}_{\text{re}}(-|\Delta\mu|), \quad (11)$$

$$\Delta s_{\text{re}}(|\Delta\mu|) = \mathbf{s}_{\text{tr}}(|\Delta\mu|) - \mathbf{s}_{\text{tr}}(-|\Delta\mu|), \quad (12)$$

where  $\mathbf{s}_{\text{re/tr}}(\Delta\mu)$  are the intersections of the corresponding outgoing asymptotes with the step edge. (For wide steps we take the intersections between the asymptotes and the centre line of the step.) Since the outgoing trajectory asymptotes for opposite staggered sublattice potentials ( $\pm|\Delta\mu|$ ) are roughly parallel,  $\Delta s_{\text{tr}}(|\Delta\mu|)$  and  $\Delta s_{\text{re}}(|\Delta\mu|)$  are well defined and can be interpreted as shown in Fig. 1 (a).

Figure 5 displays the shifts of wave packets coming in at normal incidence ( $\alpha = 0$ ), with reflected and transmitted portions going out on likewise normal but shifted trajectories. The lateral displacements of the outgoing paths clearly reflect the two transmission regimes discussed above. Let us focus first on the left-hand side panels, where the wave packet energy is  $E = 0.2t$ , and the wave packet size is fixed at  $\sigma_k = 0.1/a$ . For low step heights  $V_0 \lesssim V_c$  [Fig 5 (a)], where intravalley transmission is favoured, the lateral shifts of the transmitted trajectories (solid lines) are small compared to those of the reflected trajectories (dashed lines) for both sharp (black dots) and smooth (red triangles) potential steps. For larger step heights  $V_0 > V_c$  [panel (b)], where intervalley reflection dominates, the behaviour of the trajectory shifts reverses, with the largest lateral displacements occurring for the transmitted wave packet portion. In the present cases the largest shifts are  $\sim 40a$ , which is of the order of the real space wave packet diameter at impact onto the step edge ( $\sim 2\sigma_k^{-1} = 20a$ ).

Panels (a) and (b) further suggest that steepening the potential steps strongly reduces the lateral shifts of the reflected paths. This finding goes beyond the semiclassical analytical approximation, which relies on smooth potentials<sup>25,46</sup> and upon integration of Eq. (1) predicts

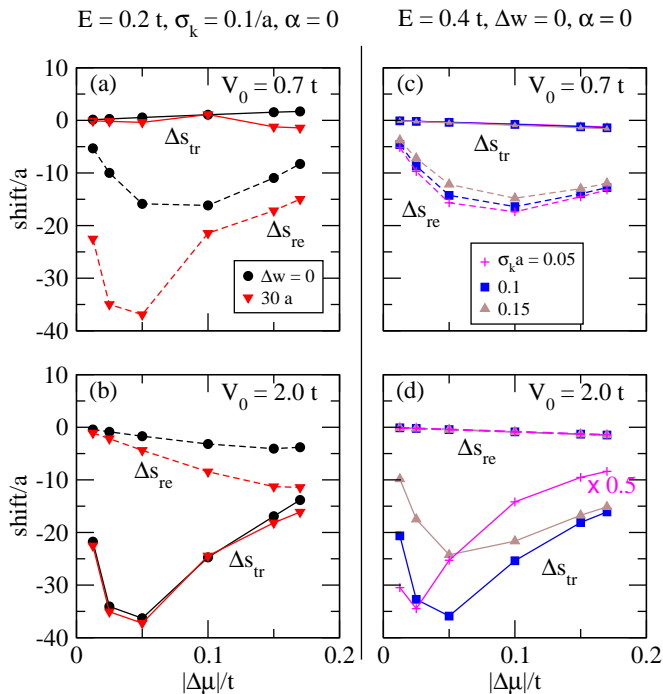


FIG. 5. (Color online) Lateral shifts of the transmitted (solid lines) and the reflected (dashed lines) wave packet trajectories for normal incidence ( $\alpha = 0$ ) as a function of staggered sublattice potential  $\Delta\mu$ . The panels (a) and (b) display the shifts of wave packets with energy  $E = 0.2t$  ( $V_c = 1.2t$ ) for step heights  $V_0 = 0.7t$  and  $2.0t$ , respectively, for two step widths ( $\Delta w = 0, 30a$ ). Panels (c) and (d) show the trajectory shifts for a sharp step ( $\Delta w = 0$ ) with  $V_0 = 0.7t$  and  $2.0t$ , respectively, and different wave packet sizes  $\sigma_k$ ; here the wave packet energy is  $E = 0.4t$  ( $V_c = 1.4t$ ). In (d) the  $\sigma_k = 0.05/a$  curve has been reduced by a factor of 0.5.

that

$$\Delta s_{\text{re}} \approx - \int_{\mathbf{k}_{\text{in}}}^{\mathbf{k}_{\text{re}}} d\mathbf{k} \times \hat{\Omega}_{\mathbf{k}}^+ \quad (13)$$

is independent of the underlying potential shape ( $\mathbf{k}_{\text{in}}$  and  $\mathbf{k}_{\text{re}}$  are the central momenta of the initial wave packet and the reflected wave packet portion, respectively).<sup>34</sup> Nonetheless, Eq. (13) further suggests that in the intravalley regime  $V_0 \lesssim V_c$  the reflected (transmitted) shifts  $\Delta s_{\text{re}}$  ( $\Delta s_{\text{tr}}$ ) are large (small), due to constructive (destructive) integration of the Berry curvature within the same band (in different bands). The opposite is true for the intervalley regime  $V_0 \gtrsim V_c$  such that  $\Delta s_{\text{tr}} > \Delta s_{\text{re}}$ . The shifts reflect the topological properties of the Bloch states, which can be manipulated valley-selectively in graphene-like materials such as silicene by applying a perpendicular electric field and/or photo-irradiation.<sup>9,10</sup>

It is also interesting to observe that the reflected shifts are maximized for moderate  $\Delta\mu$ . The maximum shifts are especially pronounced for the reflected (transmitted) trajectories in panel (a) [(b)]. Furthermore, extrapolating to  $\Delta\mu = 0$  all shifts seem to disappear. This suggests that higher order corrections (such as the second order

term discussed in Ref. 31) due to a sharp, discontinuous potential are absent for  $\Delta\mu = 0$  in spite of the broken inversion symmetry originating from the armchair step edge.

To study the effect of the wave packet size on the lateral shifts, we have considered wave packets at normal incidence and at a slightly higher energy  $E = 0.4t$ . A higher energy moves the initial central momentum further away from the Dirac point  $K'$ . This allows larger variation of the momentum space wave packet size  $\sigma_k$  without creating highly dispersive real space wave packets that appear when  $K'$  is included in the momentum space support.<sup>37</sup> Here we also focus on sharp steps only ( $\Delta w = 0$ ). The resulting lateral shifts are displayed in Fig. 5 (c) and (d) representing both Klein tunneling regimes  $V_0 \lesssim V_c$  and  $\gtrsim V_c$  with  $V_c = 1.4t$ , respectively. The overall behaviour is similar to the low energy wave packet shifts at  $E = 0.2t$  for sharp steps [cf. black curves with dots in (a) and (b)]. While the transmitted (reflected) shifts are largely unaffected by variation of  $\sigma_k$  for  $V_0 \lesssim V_c$  ( $\gtrsim V_c$ ), the reflected (transmitted) shifts increase with decreasing momentum wave packet size  $\sigma_k$  (i.e. with increasing initial real space wave packet size). This indicates that semiclassical approximations of wave packet shifts like Eq. (13) are corrected and significantly weighted by the overall wave packet and Berry curvature distributions in momentum space.

#### IV. VALLEY HALL EFFECT AND BLOCH OSCILLATIONS

A sharp or smooth step imposes an electric field locally. In the opposite limit of a uniform electric field, Berry curvature induced shifts can also be observed in the wave packet motion.<sup>34</sup> In the presence of a uniform electric field along the  $\Gamma$ -K direction, electron wave packets perform Bloch oscillations in real space and periodically pass through K and  $K'$  valleys in momentum space. Near K and  $K'$  interband Bloch-Zener transitions redistribute the wave packet weights in both bands such that in real space an initially one component wave packet splits up into two opposite oscillating wave packets. By including a finite Berry curvature, the trajectories are laterally shifted at each pass through a valley. This is the semiclassical manifestation of the valley Hall effect.<sup>25,34</sup>

The resulting trajectories are shown in Fig. 2 for a uniform electric field of magnitude  $F = 0.015t/(|e|a)$  oriented normally to the armchair direction. Here the initial Gaussian-like wave packet is centred at the  $\Gamma$  point ( $\mathbf{k}_0 = \mathbf{0}$ ) with full weight of the wave function given to the electron band.<sup>47</sup> The real space and momentum space positions of the wave packet at intermediate points during one oscillation period are indicated by the numbers in Fig. 2 for the red solid ( $\mu = 0.1t$ ) trajectory pair. Panel (b) of Fig. 6 displays the corresponding temporal

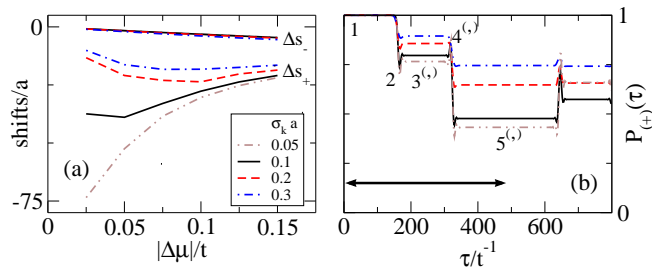


FIG. 6. (Color online) Lateral shifts and interband Bloch-Zener transitions associated with Bloch oscillations / valley Hall effect for the parameters used in Fig. 2. (a) Lateral shifts for various (initial) wave packet sizes  $\sigma_k$  as a function of staggered sublattice potential  $|\Delta\mu|$ ; the shifts are indicated in Fig. 2. (b) Electron band weight of the oscillating wave packets as a function of time  $\tau$ . The jumps correspond to Bloch-Zener transitions at the Dirac points. The black double arrow indicates one Bloch oscillation period. The numbers correspond to the temporal sequence displayed in Fig. 2. Please see main text for details.

evolution of the wave packet's electron band weight

$$P_{(+)}(\tau) = \sum_{\mathbf{k}} \rho^{(+)}(\mathbf{k}; \tau), \quad (14)$$

with the numbers corresponding to those in Fig. 2. During one oscillation period (sequence 1  $\rightarrow$  5<sup>(i)</sup>) the wave packet is driven through the K' and the K valley. Each time the wave packet passes through a valley (points 2 and 4), a portion undergoes a Bloch-Zener transition from the electron band to the hole band [and vice versa], splitting the wave packet in real space due to the opposite group velocities. The interband portion's velocity in real space remains roughly unchanged (i.e., continues from point 2 of the lower red solid trajectory to point 3' of the upper red solid trajectory in Fig. 2), while the intraband part's velocity reverses its sign (i.e., propagates from point 2 to 3 on the lower red solid trajectory). During the valley passage, the intraband portion of the wave packet experiences a Berry curvature induced side shift. The shift of the interband portion on the other hand is minute. Both types of lateral shifts are indicated in Fig. 2, where  $\Delta s_+$  ( $\Delta s_-$ ) stands for the intraband (interband) valley Hall shift, respectively, and quantified in Fig. 6 (a) for various initial wave packet sizes  $\sigma_k$ . The behavior of the shifts  $\Delta s_+$  and  $\Delta s_-$  is in agreement with that of  $\Delta s_{re}$  and  $\Delta s_{tr}$  in the case of the step potential, respectively. Interestingly, as before, the shifts are largest for small  $\sigma_k$  (i.e., for large initial real space wave packet sizes). In the limit of an extended Bloch wave, trajectories and shifts are not defined but a phase slip in the wave function portions may be expected due to the finite Berry curvature. We also note, that, as implied by Eq. (13) and despite the  $\sigma_k$ -dependence, the shifts are largely independent of the field strength  $|\mathbf{F}|$ .

The Bloch-Zener transitions causing the jumps in Fig. 6 (b) are suppressed for large gaps and for small driving forces. For these reasons the jumps at the first two

transitions (at  $\tau \approx 160/t$  and  $320/t$ ) are largest for wave packets with small  $\sigma_k$  as most of the wave packet experiences only a small gap at the Dirac point. At later jumps the wave packet has contributions and transitions from and to both bands, so that after long times one expects  $P_+(\tau) = 0.5$ .

## V. SUMMARY AND CONCLUSION

We have investigated in detail the semiclassical electron dynamics in graphene using a numerical wave packet simulation. Compared to the semiclassical analytical approach<sup>25,31</sup> the numerical simulations are more general and in principle exact. They are based on the full graphene tight-binding Hamiltonian and can account for intervalley, interband and Berry phase related phenomena.

The present simulations establish both intra- and intervalley Klein tunneling processes. The latter becomes relevant for sufficiently tall potential steps and has received only limited attention in graphene-based Klein tunneling studies. In this limit, intervalley transmission is greatly enhanced in the presence of a finite gap and/or by smoothing the step profile due to the lack of pseudospin conservation. The presence of a gap furthermore leads to notable Berry curvature induced trajectory shifts, which for the cases considered, are roughly of the order of the wave packet size. Such trajectory modifications are reminiscent of the Hall effect of light in three dimensions, where an electromagnetic wave packet scatters at an interface between two optically different media. Here reflected and transmitted light rays are similarly laterally shifted at the interface due to Berry curvature corrections.<sup>32,33</sup>

Applying a linear potential, our simulations illustrate the valley Hall effect in form of laterally shifted Bloch oscillation trajectories.<sup>34</sup> Accompanying Bloch-Zener transitions redistribute the wave function among the graphene bands, hence giving rise to two wave function portions with opposite oscillating motion in real space.

The present study highlights valley-dominated scattering dynamics of electrons in a honeycomb lattice. The energy bands and valley properties of silicene, a close relative of graphene, have been suggested to be easily manipulable experimentally; in fact, they may be tuned to exhibit a variety of topological properties, ranging from single Dirac-cone states to various types of quantum Hall insulators.<sup>10</sup> Such manipulations would have direct impact on the intra- and intervalley wave packet dynamics discussed here.

The simulation results also make explicit the dependence of the trajectory shifts on the wave packet size and the effective mass (i.e. the Berry curvature distribution in momentum space). Reducing the initial momentum space wave packet size ( $\sigma_k$ ) can drastically enhance the trajectory shifts in both regimes. Furthermore, for a fixed

wave packet size, there is an optimum effective mass that maximizes the shifts of the outgoing trajectories and the widths of the Bloch oscillation paths.

Experimentally, the trajectory shifts may be observed as scattering asymmetry at np junctions<sup>15,18,19</sup> for either reflected or transmitted electrons, where a staggered sublattice potential may originate from an appropriate substrate material or, in the case of silicene and germanene, from an external perpendicular electric field.<sup>9,10</sup> In the limit of a single spatially extended Bloch state, Berry curvature induced shifts become phase jumps at the step interface, which may be observed as anomalies in the conductance oscillations across a potential barrier due to interference between forward and backward reflected wave functions.<sup>16</sup> These shifts may also substantially affect the electron focusing and lensing behaviour of potential barriers and potentials steps in electron optics

applications.<sup>48</sup>

It would further be interesting to investigate how the wave packet dynamics change for zigzag and Klein edges. The dynamics at zigzag and Klein edges are less symmetric about the interface normal than in the armchair case. For sharp steps this will affect the direction and the Berry curvature induced shifts of the wave packet trajectories. The coupling of wave packets with edge states may give rise to further intriguing behavior at resonance energies.

The authors thank T. Nakanishi, K. Wakabayashi, N. Kumada, O. Entin-Wohlman and A. Aharony for useful discussions. Y. H. acknowledges partial financial support through Grants-in-Aid (KAKENHI No. 23340112 and No. 23654128) from JSPS. Part of this work is supported financially by the Funding Program for World-Leading Innovative R&D Science and Technology (FIRST).

- 
- \* cpuetter@comas.frsc.tsukuba.ac.jp
- 1 A. H. Castro Neto, F. Guinea, N. M. R. Peres, K. S. Novoselov and A. K. Geim, *Rev. Mod. Phys.* **81**, 109 (2009).
  - 2 K. S. Novoselov, A. K. Geim, S. V. Morozov, D. Jiang, M. I. Katsnelson, I. V. Griegorieva, S. V. Dubonos, and A. A. Firsov, *Nature* **438**, 197 (2005).
  - 3 Y. Zhang, Y.-W. Tan, H. L. Stormer, and P. Kim, *Nature* **438**, 201 (2005).
  - 4 Y. Hatsugai, T. Fukui, and H. Aoki, *Phys. Rev. B* **74**, 205414 (2006).
  - 5 N. Nagaosa, J. Sinova, S. Onoda, A. H. MacDonald, and N. P. Ong, *Rev. Mod. Phys.* **80**, 1083 (2010).
  - 6 K. Takeda and K. Shiraishi, *Phys. Rev. B* **50**, 14916 (1994).
  - 7 B. Lalmi, H. Oughaddou, H. Enriquez, A. Kara, S. Vizzini, B. Ealet, and B. Aufray, *Appl. Phys. Lett.* **97**, 223109 (2010).
  - 8 P. De Padova *et al.*, *Appl. Phys. Lett.* **96**, 261905 (2010).
  - 9 C.-C. Liu, H. Jiang, and Y. Yao, *Phys. Rev. B* **84**, 195430 (2011).
  - 10 M. Ezawa, *Phys. Rev. Lett.* **110**, 026603 (2013).
  - 11 O. Klein, *Z. Phys.* **53**, 157 (1929).
  - 12 J. R. Williams, L. DiCarlo, and C. M. Marcus, *Science* **317**, 638 (2007).
  - 13 B. Huard, J. A. Sulpizio, N. Stander, K. Todd, B. Yang, and D. Goldhaber-Gordon, *Phys. Rev. Lett.* **98**, 236803 (2007).
  - 14 R. V. Gorbachev, A. S. Mayorov, A. K. Savchenko, D. W. Horsell, and F. Guinea, *Nano Lett.* **8**, 1995 (2008).
  - 15 N. Stander, B. Huard, and D. Goldhaber-Gordon, *Phys. Rev. Lett.* **102**, 026807 (2009).
  - 16 A. F. Young, and P. Kim, *Nat. Phys.* **5**, 222 (2009).
  - 17 K. J. A. Reijnders, T. Tudorovskiy, and M. I. Katsnelson, *Ann. Phys.* **333**, 155 (2013).
  - 18 R. N. Sajjad, S. Sutar, J. U. Lee, and A. W. Gosh, *Phys. Rev. B* **86**, 155412 (2012).
  - 19 A. Rahman, J. W. Guikema, N. M. Hassan, and N. Markovic, arXiv:1304.5533 (2013).
  - 20 K. F. Mak, C. Lee, J. Hone, J. Shan, and T. F. Heinz, *Phys. Rev. Lett.* **105**, 136805 (2010).
  - 21 D. Xiao, G.-B. Liu, W. Feng, X. Xu, and W. Yao *Phys. Rev. Lett.* **108**, 196802 (2012).
  - 22 T. Cao, G. Wang, W. Han, H. Ye, C. Zhu, J. Shi, Q. Niu, P. Tan, E. Wang, B. Liu, and J. Feng, *Nat. Commun.* **3**, 887 (2012).
  - 23 K. F. Mak, K. He, J. Shan, and T. F. Heinz, *Nature Nanotech.* **7**, 494 (2012).
  - 24 K. F. Mak, K. L. McGill, J. Park, and P. L. McEuen, *Science* **344**, 1489 (2014).
  - 25 D. Xiao, M.-C. Chang, and Q. Niu, *Rev. Mod. Phys.* **82**, 1959 (2010), and references therein.
  - 26 M.-C. Chang and Q. Niu, *J. Phys.: Condens. Matter* **20**, 193202 (2008), and references therein.
  - 27 M. I. Katsnelson, K. S. Novoselov, and A. K. Geim, *Nat. Phys.* **2**, 620 (2006).
  - 28 V. V. Cheianov and V. I. Fal'ko, *Phys. Rev. B* **74**, 041403 (2006).
  - 29 N. M. R. Peres, *J. Phys.: Condens. Matter* **21**, 323201 (2009).
  - 30 P. E. Allain and J. N. Fuchs, *Eur. Phys. J. B* **83**, 301 (2011).
  - 31 Y. Gao, S. A. Yang, and Q. Niu, arXiv:1402.2538v1 (2014).
  - 32 M. Onoda, S. Murakami, and N. Nagaosa, *Phys. Rev. Lett.* **93**, 083901 (2004).
  - 33 M. Onoda, S. Murakami, and N. Nagaosa, *Phys. Rev. E* **74**, 066610 (2006).
  - 34 R. B. Diener, G. Sundaram, Q. Niu, A. M. Dudarev, arXiv:cond-mat/030618v1 (2003).
  - 35 M. Suzuki, *Phys. Lett. A* **146**, 319 (1990).
  - 36 M. Suzuki, *J. Phys. Soc. Jpn.* **61**, 3015 (1992).
  - 37 The initial wave packet has the form  $\Psi_{\mathbf{k}_0, \sigma_k, \mathbf{r}_0}^{(+)} = U(\Delta\tau) [1 + \cos(\pi|\mathbf{k} - \mathbf{k}_0|/\sigma_k)] \exp(-i\mathbf{k} \cdot \mathbf{r}_0) \Theta(\sigma_k - |\mathbf{k} - \mathbf{k}_0|)$ , where  $\mathbf{r}_0$  is a suitable point on the step edge, roughly defining the impact point, and  $\Theta(x)$  denotes the Heaviside step function. The cosine term approximates a Gaussian and is preferred over a Gaussian shape as its momentum space support is finite. The parameters  $\mathbf{k}_0$  and  $\sigma_k$  can be chosen such that the Dirac point lies outside the wave function's support, which otherwise would lead to a drastic dispersion of the wave packet in all directions in real space. To evolve the wave packet back in time to a starting position away from the step edge, the wave function is multiplied by



the phase factor  $U(\Delta\tau) = \exp[-i\Delta\tau \varepsilon(\mathbf{k})]$ , where  $\varepsilon(\mathbf{k}) = [\Delta\mu^2 + |\Delta(\mathbf{k})|^2]^{1/2}$  with  $|\Delta(\mathbf{k})|^2 = [1 + 4\cos^2(\sqrt{3}ak_y/2) + 4\cos(3ak_x/2)\cos(\sqrt{3}ak_y/2)]$  denotes the gapped electron band dispersion. Here we used  $\Delta\tau = -150t^{-1}$  for all Klein tunneling simulations.

<sup>38</sup> M. I. Katsnelson, Eur. Phys. J. B **57**, 225 (2007).

<sup>39</sup> T. M. Rusin and W. Zawadzki, Phys. Rev. B **76**, 195439 (2007).

<sup>40</sup> J. Cserti and G. David, Phys. Rev. B **82**, 201405 (2010).

<sup>41</sup> G. M. Maksimova, V. Ya. Demikhovskii, and E. V. Frolova, Phys. Rev. B **78**, 235321 (2008).

<sup>42</sup> C. Zener, Proc. R. Soc. Lond. A **137**, 696 (1932).

<sup>43</sup> C. Wittig, J. Phys. Chem. B **109**, 8428 (2005).

<sup>44</sup> J.-N. Fuchs, Phys. Rev. A **86**, 063613 (2012).

<sup>45</sup> A. M. Dudarev, R. B. Diener, I. Carusotto, and Q. Niu, Phys. Rev. Lett. **92**, 153005 (2004).

<sup>46</sup> M. C. Chang and Q. Niu, Phys. Rev. B **53**, 7010 (1996).

<sup>47</sup> For the semiclassical valley Hall effect, the initial wave packet takes the form  $\Psi_{0,\sigma_k,r_0}^{(+)}(\mathbf{k}) = [1 + \cos(\pi|\mathbf{k}|/\sigma_k)]\Theta(\sigma_k - |\mathbf{k}|)$ .

<sup>48</sup> V. V. Cheianov, V. I. Fal'kov, and B. L. Altshuler, Science **315**, 1253 (2007).